

Optical Modulators

Edgar A. Peralta*, Alireza Marandi, and Alok Vasudev

Department of Applied Physics, Stanford University, Stanford, CA 94305, USA

*Corresponding author: eperalta@stanford.edu

Compiled July 20, 2010

The electro- and magneto-optic effects in a LiNbO₃ crystal are characterized. In particular, we set up an amplitude modulator with a half-wave voltage of 1005V and confirmed the Bessel function dependence of the modulated sideband amplitudes when the device is operated as a phase modulator. We've observed the Faraday effect with a net polarization rotation of up to 50° and measured a Verdet coefficient of 9.6x10⁻⁵ rad/G cm. We also investigate the performance of a commercial acousto-optic modulator(AOM) that uses a dense flint glass as the optical medium. The AOM is used to deflect a beam through an angle of 14mrad (~106 resolvable spots) across its 100MHz bandwidth. The periodic exchange of power between the undeflected and diffracted beam as the acoustic intensity increases is also observed. © 2010 Optical Society of America

1. Introduction

The ability to modify a material's dielectric tensor by means of applied heat, electric, magnetic or acoustic fields provides a convenient way to control the phase or intensity of the light propagating through the material. This modulation has many useful applications such as impression of information onto optical beams for telecommunications, Q-switching of lasers or optical beam deflection.

It was shown in a previous paper [1] that an anisotropic material can have non-equal permittivity eigenvalues which can lead to different field polarization components experiencing different indices of refraction, thus accruing a different phase and rotating the state of polarization, depending on the propagation direction.

The effect of an applied field can be treated as a perturbation to the dielectric tensor, $\bar{\epsilon} = \bar{\epsilon}_0 + \overline{\Delta\epsilon}$, where the relationship between $\overline{\Delta\epsilon}$ and the applied field depends on the interaction taking place. In the following sections, we examine the specifics of the electro-, magneto-, and acousto-optic interactions and compare our experimental data with theory.

2. Electro-Optic Modulation

The case of an applied *electric* field is usually treated using the impermeability tensor instead, $\bar{\mathbf{b}} = \epsilon^{-1}$, with the interaction characterized by:

$$\Delta b_{ij} = \sum_{k=x,y,z} r_{ijk} E_k, \quad (1)$$

where $\bar{\mathbf{b}}$ is the second order, *electro-optic* tensor which can be written as a 2D (6x3) matrix in contracted notation¹ due to the symmetry of $\bar{\mathbf{b}}$ for a lossless crystal.

For LiNbO₃ for example [2],

$$\overline{\Delta\mathbf{b}} = \begin{pmatrix} 0 & -r_{22} & r_{13} \\ 0 & r_{22} & r_{13} \\ 0 & 0 & r_{33} \\ 0 & r_{42} & 0 \\ r_{42} & 0 & 0 \\ -r_{22} & 0 & 0 \end{pmatrix} \begin{bmatrix} E_x \\ E_y \\ E_z \end{bmatrix} = \begin{pmatrix} -r_{22}E_y + r_{13}E_z \\ r_{22}E_y + r_{13}E_z \\ r_{33}E_z \\ r_{42}E_y \\ r_{42}E_x \\ -r_{22}E_x \end{pmatrix},$$

¹ $r_{ijk} \rightarrow r_{lk}$, where $l = 1 - 6$ for $ij = 11, 22, 33, 23, 13, 23$.

and choosing the applied field as $\mathbf{E} = E_a \hat{z}$, one has:

$$\bar{\mathbf{b}} = \begin{pmatrix} 1/n_o^2 + r_{13}E_a & 0 & 0 \\ 0 & 1/n_o^2 + r_{13}E_a & 0 \\ 0 & 0 & 1/n_e^2 + r_{33}E_a \end{pmatrix} \quad (2)$$

which leaves the principal axes unchanged. The material remains uniaxial but now the indices have a linear dependence on the applied field:

$$\begin{aligned} n_o(E_a) &\approx n_o - \frac{1}{2}n_o^3 r_{13} E_a \\ n_e(E_a) &\approx n_e - \frac{1}{2}n_e^3 r_{33} E_a \end{aligned} \quad (3)$$

One can build an amplitude modulator if the propagating field is polarized at some angle to the eigenpolarizations. The two polarization components pick up different phases, rotate the polarization state, and a polarizer after the crystal attenuates the field by an amount proportional to the applied field. A field propagating in LiNbO₃ along the *x*- or *y*-axis, polarized at 45° to *z*-axis picks up a relative phase shift of $\Delta\phi = 2\pi[(n_e - n_o) - \frac{1}{2}(n_e^3 r_{33} - n_o^3 r_{13})E_a]L/\lambda$. If the crystal dimension along the *z*-axis is *d*, then the applied field is $E_a = V_a/d$, and the voltage required to incur a phase of π (half-wave) is

$$V_{1/2} = \frac{\lambda}{n_e^2 r_{33} - n_o^2 r_{13}} \frac{d}{L} \quad (4)$$

We setup an amplitude modulator with a LiNbO₃ crystal between crossed polarizers and measured the transmitted power from a He-Ne laser as a voltage was applied across the crystal's *x*-axis. The data illustrated in figure 1 shows the expected sinusoidal output as the beam's linear polarization is rotated about the propagation axis. The measured half-wave voltage from this modulator arrangement was 1004.6 V, which is within the expected range of values given by equation 4 for LiNbO₃ at 633nm: $V_{1/2} = 2810.6(d/L)$. Unfortunately we only measured the crystal's length (1cm) so a theoretical value cannot be calculated, however, a required

crystal height of 3.6 mm is certainly likely given the modulator's 2mm aperture.

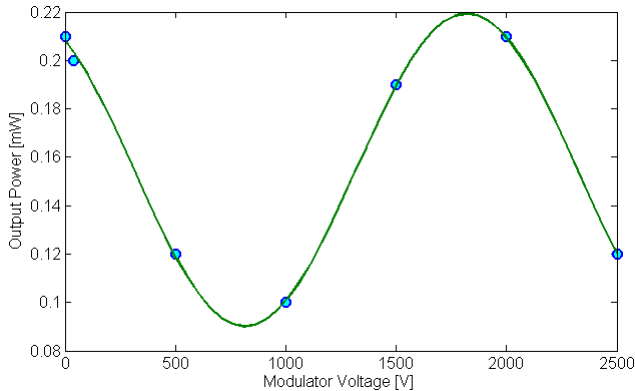


Fig. 1. Transmission through amplitude modulator versus modulator voltage.

Alternatively, if one propagates a field polarized along one of the crystal's eigenpolarizations, then one can modulate the phase without altering the polarization (and possibly the amplitude if any polarizers are present). The accrued phase is given by $\Delta\phi_i = 2\pi n_i(E_a)L/\lambda$, where L is the crystal length. If the applied field is sinusoidal, $E_a(t) = E_a \sin w_m t$, then the resulting phase-modulated field has the form $E = E_o e^{i(\omega t + \phi_o - \delta_i \sin w_m t)}$, which can be written as:

$$E = E_o e^{i\phi_o} \sum_n J_n(\delta_i) e^{i(\omega + n w_m)t}, \quad (5)$$

with a modulation index is given by

$$\delta_i = (\pi n_i^3 r_{i3}/\lambda)(L/d)V_a \quad (6)$$

This expression shows that the energy is distributed in sidebands with Bessel function amplitudes that vary as a function of the modulation index $\delta_i(V_a)$.

We adjusted the polarizer before the crystal to ensure the input polarization was along one of the crystal's eigenpolarizations and drove the modulator with an RF-amplified signal at 100MHz from a function generator. We then filtered the output to reject the fundamental and measured the sideband amplitude as a function of modulator voltage. The result is shown in figure 2 and shows good agreement with a fit to the square of the sideband Bessel amplitudes of equation 5. The fit results in a modulation index of $.0027 V_a$, which doesn't exactly match the expected $.0046 V_a$ from equation 6 for polarization along \hat{z} , but is at least between this value and that for modulation of a beam polarized along \hat{y} of $.0014 V_a$. This indicates that the input polarization wasn't exactly along one of the eigenpolarizations.

3. Magneto-Optic Modulation

In the case of an applied *magnetic* field, the interaction can be described as:

$$\Delta\epsilon_{ij} = \sum_{k=x,y,z} g_{ijk} B_k, \quad (7)$$

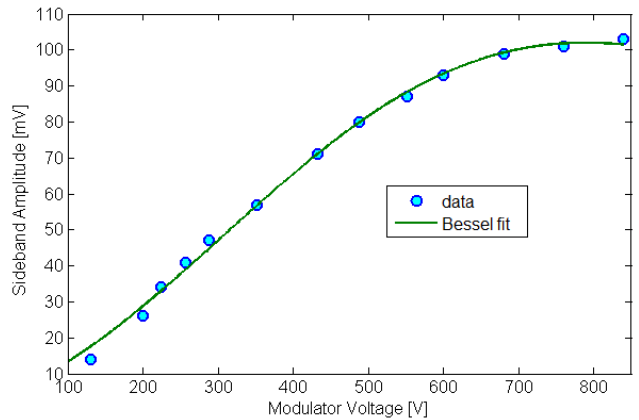


Fig. 2. Sideband amplitude of a phase-modulated beam versus modulator voltage.

where $g_{ijk} = i e_{ijk} g_k$ is the *magneto-optic* tensor, and e_{ijk} is the Levi-Cevita symbol. For an applied field $\mathbf{B} = B_a \hat{z}$ on a uniaxial crystal one then has:

$$\bar{\epsilon} = \begin{pmatrix} n_o^2 & i g_z B_a & 0 \\ -i g_z B_a & n_o^2 & 0 \\ 0 & 0 & n_e^2 \end{pmatrix} \quad (8)$$

which has a principal axes system that consists of the right and left circular polarization eigenvectors $\hat{c}_{\pm} = \frac{1}{\sqrt{2}}(1, \mp i, 0)$, and \hat{z} . A field that propagates along \hat{z} decomposes into this basis, and the two polarization components experience different indices of refraction:

$$n_{\pm}(B_a) \approx n_o \mp \frac{g_z B_a}{2n_o} \quad (9)$$

which results in a relative phase difference between the two polarization components and thus a polarization rotation. The amount of rotation can be quantified by considering a field that is initially polarized along $\hat{x} = \frac{1}{\sqrt{2}}(\hat{c}_+ + \hat{c}_-)$. After some crystal length L , the field exits polarized along

$$\frac{1}{\sqrt{2}} e^{i\phi_o} [\hat{c}_+ e^{-i\phi(B_a)} + \hat{c}_- e^{+i\phi(B_a)}] = e^{i\phi_o} \begin{bmatrix} \cos \phi(B_a) \\ -\sin \phi(B_a) \\ 0 \end{bmatrix},$$

where it is evident the polarization rotates by an angle

$$\phi(B_a) = \frac{\pi g_z B_a L}{n_o \lambda} \rightarrow \rho = \frac{d\phi}{dL} = V B_a, \quad (10)$$

with $V = \pi g_z / n_o \lambda$ as the Verdet constant. To measure this effect we aligned a LiNbO₃ to be centered on a large cylindrical permanent magnet and moved the magnet away from the crystal to vary the longitudinal magnetic field while monitoring the transmitted power after a polarizer. The magnetic field at the crystal was measured using a Tesla meter. The calculated polarization rotation as a function of applied magnetic field is shown in figure 3 to follow the expected linear relationship from

equation 10. The slope of the line yields a Verdet coefficient of $V=55.24 \text{ deg/T cm}=9.6 \times 10^{-5} \text{ rad/G cm}$, and a corresponding value of $g_z=4.4 \times 10^{-5} \text{ 1/T}$, which justifies the approximation for equation 9.

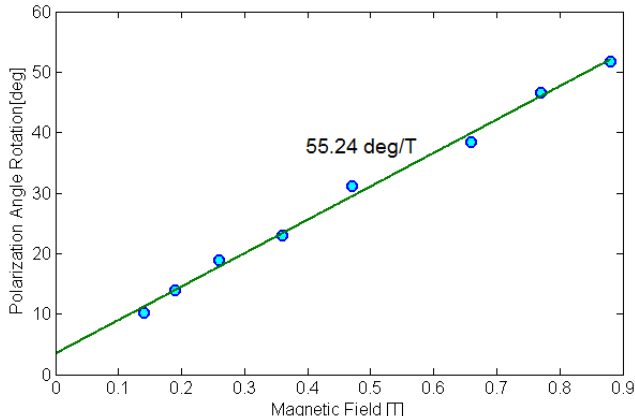


Fig. 3. Faraday Effect: polarization rotation as a result of applied magnetic field.

4. Acousto-Optic Modulation

In the case of an applied *acoustic* field, the interaction can be described as:

$$\Delta b_{ij} = \sum_{k=x,y,z} p_{ijkl} S_{kl}, \quad (11)$$

where p_{ijkl} is the photo-elastic (4th rank) tensor and S_{kl} is the elastic strain. For LiNbO_3 , p_{ijkl} in reduced subscript notation is [2]:

$$\bar{\mathbf{p}} = \begin{pmatrix} p_{11} & p_{12} & p_{13} & p_{14} & 0 & 0 \\ p_{12} & p_{11} & p_{13} & -p_{14} & 0 & 0 \\ p_{31} & p_{31} & p_{33} & 0 & 0 & 0 \\ p_{41} & -p_{41} & 0 & p_{44} & 0 & 0 \\ 0 & 0 & 0 & 0 & p_{44} & p_{41} \\ 0 & 0 & 0 & 0 & p_{14} & p_{44} \end{pmatrix}$$

The elastic strain is related to the displacement gradients as:

$$S_{kl} = \frac{1}{2} \left(\frac{\partial \mu_i}{\partial x_j} + \frac{\partial \mu_j}{\partial x_i} \right),$$

so considering an acoustic wave along the z -axis, $\mu = u e^{i(w_a t - k_a z)} \hat{z}$, we see that the only nonzero term is $S_3 = S_{zz} = S_a e^{i(w_a t - k_a z)}$, with $S_a = -i k_a u$ and the resulting impermeability tensor from equation 11 takes on the same form as that of equation 2 but with $p_{i3} S_3$ instead of $r_{i3} E_a$. Inverting, we get

$$\Delta \epsilon_{ii} \approx -p_{i3} n_i^4 S_a e^{i(w_a t - k_a z)}, \quad (12)$$

which, from the slowly varying envelope approximation to the wave equation:

$$ik \frac{\partial \mathbf{A}}{\partial \rho} e^{i(\omega t - \mathbf{k} \cdot \mathbf{r})} = \frac{\omega^2}{c^2} (\overline{\Delta \epsilon} \cdot \mathbf{E}), \quad (13)$$

we see can cause propagation at different frequencies and along different wavevectors. These new waves are essentially diffracted from the grating setup by the acoustic wave. Combining equations 12 and 13 we can calculate how these fields evolve:

$$\begin{aligned} \frac{\partial A_i}{\partial \rho_i} &= i \gamma A_d e^{i(w_d \pm w_a - w_i)t} e^{-i(\mathbf{k}_d \pm \mathbf{k}_a - \mathbf{k}_i) \cdot \mathbf{r}}, \\ \frac{\partial A_d}{\partial \rho_d} &= i \gamma A_i e^{i(w_d \pm w_a - w_i)t} e^{+i(\mathbf{k}_d \pm \mathbf{k}_a - \mathbf{k}_i) \cdot \mathbf{r}}, \end{aligned} \quad (14)$$

with a coupling coefficient $\gamma = -\pi p_{13} n_l^3 S_a / 2\lambda$, for an l -axis polarized incident wave. If the argument in the exponentials is non-zero, the average of these derivatives vanishes and no diffracted waves are generated. We must then have $\mathbf{k}_d = \mathbf{k}_i \pm \mathbf{k}_a$, which is the Bragg condition, as well as $w_d = w_i \pm w_a$ which is simply energy conservation. Since $w_i \gg w_a$, $w_d \approx w_i = w$ and $k_d \approx k_i = k$, the Bragg condition gives $2k \sin \theta_B = k_a$, where θ_B is the Bragg angle between the incident wave and the acoustic wavefronts. The deflection angle between the two waves is then $2\theta_B$, and since $\lambda_a f_a = v_a$, where f_a is the acoustic frequency and v_a is the acoustic speed in the material, we have:

$$\theta_{\text{def}} = \lambda f_a / n v_a \quad (15)$$

To verify this, we used a commercial AOM (IntraAction AOM-80) which uses a dense flint glass as the optical medium and measured the deflection of a He-Ne laser beam a few meters away as a function of driving frequency. The results are plotted in figure 4 which shows the expected linear dependence with a slope of .147 mrad/MHz, which is close to the calculated value of .11 mrad/MHz from equation 15.

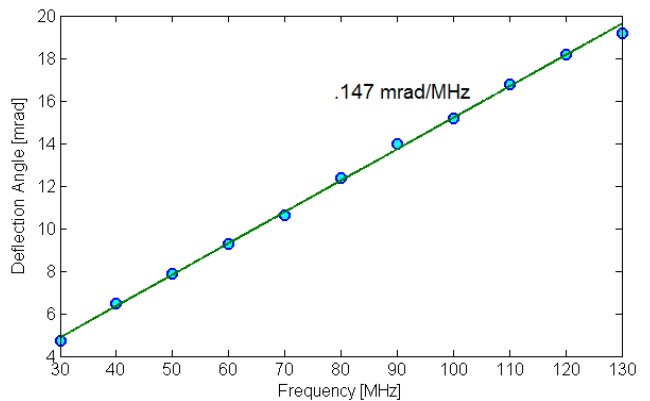


Fig. 4. Deflection of first order diffracted beam versus modulator frequency.

The absolute deflection in going from 30 to 130 MHz was 14 mrad and an estimate of the diffraction angle gives $\theta_{\text{dif}} = \lambda/nD \approx .131 \text{ mrad}$, using an estimated beam diameter of $D=3\text{mm}$. This results in a total of 106 resolvable spots that can be observed over this frequency range.

We also measured the transmitted power of the 0th order (non-diffracted) beam as a function of modulator

voltage at a constant modulation frequency of 40MHz. The results are shown in figure 5.

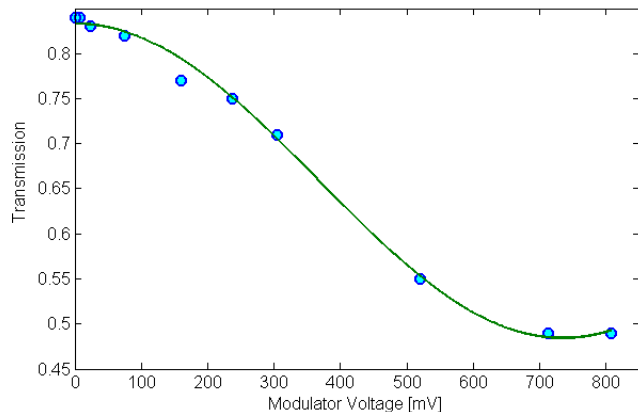


Fig. 5. Transmitted power of the 0th order beam as function modulator voltage.

The transmitted power exhibits a sinusoidal variation which is what we expect since the power oscillates between the undeflected and diffracted waves as the acoustic intensity increases. This can be seen with the help of equation 14, which when the Bragg condition is met, can be solved to give

$$\begin{aligned} A_d(\rho) &= iA_i(0) \sin(\gamma \cos \theta_B \rho) \\ A_i(\rho) &= A_i(0) \cos(\gamma \cos \theta_B \rho) \end{aligned} \quad (16)$$

From this measurement we can calculate a diffraction efficiency of at most 40% which is considerably lower than the spec value of 70%. A possible reason for this is that the all other light sources, in particular the first order diffracted beam, weren't properly blocked from the detector, resulting in higher values of the transmission at higher voltages.

As a last experiment, we measured the diffraction efficiency of the modulator as a function of frequency. This was done by spatially filtering the output so that only the first order diffraction could be measured and shifting the detector to the new diffracted spot position as the modulator frequency is increased. This measurement was performed first without altering the orientation of the modulator, and repeated with the modulator realigned to obtain the proper Bragg angle at each frequency. The results are shown in figure 6.

It is evident that it is important to align the laser and acoustic beam as the modulator frequency is changed in order to phase-match properly (achieve Bragg condition) and maximize efficiency. The measured FWHM bandwidth in this case was ~ 70 MHz.

5. Conclusion

We have investigated a number of optical modulator arrangements. Applying a voltage across a LiNbO₃ crystal we setup an amplitude modulator with a half-wave

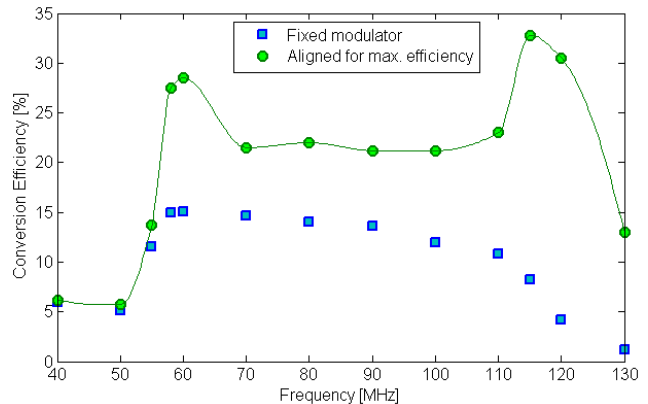


Fig. 6. Diffraction Efficiency as a function of modulator driving frequency.

voltage of 1005V and confirmed the Bessel function dependence of the modulated sideband amplitudes when the device is operated as a phase modulator. We've also observed the Faraday effect in LiNbO₃ with a net polarization rotation of up to 50° (limited by our setup but enough to allow operation as an isolator) and measured the Verdet coefficient to be 9.6×10^{-5} rad/G cm. Lastly, we used a commercial acoustooptic modulator to deflect a beam through 14mrad, ~ 106 resolvable spots, across the modulator's frequency range of 30 to 130 MHz and verified the expected periodic exchange of power between the undeflected and diffracted beam.

References

1. E. Peralta *et al.*, *Crystal Optics and Birefringence*, AP 305 Lab1 Report, (2010)
2. R. Weis and T. Gaylord, *Lithium Niobate: Summary of Physical Properties and Crystal Structure*, Appl. Phys. A, **37** (1985)